5-2019

Transferring Power through a Magnetic Couple

Nickolas Cruz Villalobos Jr.
Linfield College

Transferring Power through a Magnetic Couple

Nickolas Cruz Villalobos Jr

A THESIS

Submitted to

The Department of Physics

LINFIELD COLLEGE

McMinnville, Oregon

In partial fulfillment of the requirements for the degree

BACHELOR OF SCIENCE

In

APPLIED PHYSICS

May 2019

THESIS COPYRIGHT PERMISSIONS

Please read this document carefully before signing. If you have questions about any of these permissions, please contact the DigitalCommons Coordinator.

Title of the Thesis:

Transferring Power through a Magnetic Couple

Author's Name: (Last name, first name)

Villalobos, Nickolas

Advisor's Name

Tianbao Xie

DigitalCommons@Linfield (DC@L) is our web-based, open access-compliant institutional repository for digital content produced by Linfield faculty, students, staff, and their collaborators. It is a permanent archive. By placing your thesis in DC@L, it will be discoverable via Google Scholar and other search engines. Materials that are located in DC@L are freely accessible to the world; however, your copyright protects against unauthorized use of the content. Although you have certain rights and privileges with your copyright, there are also responsibilities. Please review the following statements and identify that you have read them by signing below. Some departments may choose to protect the work of their students because of continuing research. In these cases, the project is still posted in the repository but content will only be accessible by individuals who are part of the Linfield community.

CHOOSE THE STATEMENT BELOW THAT DEFINES HOW YOU WANT TO SHARE YOUR THESIS. THE FIRST STATEMENT PROVIDES THE MOST ACCESS TO YOUR WORK; THE LAST STATEMENT PROVIDES THE LEAST ACCESS. CHOOSE ONLY ONE STATEMENT.

K.M.S. X I **agree** to make my thesis available to the Linfield College community and to the larger scholarly community upon its deposit in our permanent digital archive, DigitalCommons@Linfield, or its successor technology. My thesis will also be available in print at Nicholson Library and can be shared via interlibrary loan.

OR

✓ I **agree** to make my thesis available **only** to the Linfield College community upon its deposit in our permanent digital archive, DigitalCommons@Linfield, or its successor technology. My thesis will also be available in print at Nicholson Library and can be shared via interlibrary loan.

OR

✓ I **agree** to make my thesis available in print at Nicholson Library, including access for interlibrary loan.

OR

✓ I **agree** to make my thesis available in print at Nicholson Library only.

Updated April 25, 2018

NOTICE OF ORIGINAL WORK AND USE OF COPYRIGHT-PROTECTED MATERIALS:

If your work includes images that are not original works by you, you must include permissions from the original content provider or the images will not be included in the repository. If your work includes videos, music, data sets, or other accompanying material that is not original work by you, the same copyright stipulations apply. If your work includes interviews, you must include a statement that you have the permission from the interviewees to make their interviews public. For information about obtaining permissions and sample forms, see https://copyright.columbia.edu/basics/permissions-and-licensing.html.

NOTICE OF APPROVAL TO USE HUMAN OR ANIMAL SUBJECTS:

If your research includes human subjects, you must include a letter of approval from the Linfield Institutional Review Board (IRB); see https://www.linfield.edu/faculty/irb.html for more information. If your research includes animal subjects, you must include a letter of approval from the Linfield Animal Care & Use Committee.

NOTICE OF SUBMITTED WORK AS POTENTIALLY CONSTITUTING AN EDUCATIONAL RECORD UNDER FERPA:

Under FERPA (20 U.S.C. § 1232g), this work may constitute an educational record. By signing below, you acknowledge this fact and expressly consent to the use of this work according to the terms of this agreement.

BY SIGNING THIS FORM, I ACKNOWLEDGE THAT ALL WORK CONTAINED IN THIS PAPER IS ORIGINAL WORK BY ME OR INCLUDES APPROPRIATE CITATIONS AND/OR PERMISSIONS WHEN CITING OR INCLUDING EXCERPTS OF WORK(S) BY OTHERS.

IF APPLICABLE, I HAVE INCLUDED AN APPROVAL LETTER FROM THE IRB TO USE HUMAN SUBJECTS OR FROM ANIMAL CARE & USE TO USE ANIMAL SUBJECTS.

Signature *Signature redacted* Date 5/15/19

Printed Name Nickolas Villalobos

Approved by Faculty Advisor *Signature redacted* Date 5/16/2019

Updated April 25, 2018

Thesis Acceptance

Linfield College

Thesis Title: Transferring Power through a Magnetic Couple

Submitted by: Nickolas Cruz Villalobos Jr

Date Submitted: May 2019

Thesis Advisor: *Signature redacted*

Dr. Tianbao Xie

Physics Department: *Signature redacted*

Dr. Michael Crosser

Signature redacted

Dr Jennifer Heath

Abstract

Properties of several working magnetic coupled rotors have been measured and their performance compared to theoretical models. Axial magnetic couplers allow rotors to work within harsh environments, without the need for seals, proper alignment, or overload protection on a motor. The influence of geometrical parameters, such as distance from the center of the rotors, polarity arrangement, and the number of dipole pairs were experimentally tested. These results can be used to improve rotor designs, to increase strength and efficiency.

Acknowledgments

The inspiration for this project came from prior summer research with my Research Advisor, Tianbao Xie. Whom I am genuinely thankful for all the guidance in and out of the classroom. The mentorship I have received throughout my four years at Linfield College has been unparallel.

I am also grateful to my Thesis Advisor, Michael Crosser, for offering time and guidance throughout this project. Your input and suggestions have been invaluable.

I also would like to thank my the Linfield College Collaborative Research Grant for funding my research.

Dedication

I would like to first and foremost thank my mother and father, Belinda and Nick Villalobos, respectively. My path to this point in my life has been winding, and throughout every curve, you have been there to love and guide me. Truly, I would not be where I am today without your support.

I would also like to thank for sister, Azlynn Villalobos, for the quiet support she has provided. My motivation to finish continued to grow with her and my family in mind.

Table of Contents

List of Figures

List of Tables

1. Introduction

1.1 Background, Applications & Advantages

Permanent magnets have many applications in society ranging from small fridge magnets to smartphones. Through understanding the physics behind them thoroughly, new technologies involving magnets are being developed to improve existing ones. It has only been in recent years that rare-earth permanent magnets have been discovered, such as Samarium Cobalt, and Neodymium Iron Boron[12]. Such findings have led companies and scientist to perform extensive research to understand better the potential applications these magnets have to improve the efficiencies of products and other applications in electromagnetic devices [8][14][13][19].

One question addressed in this research regards the operation of magnetic couples or couplings. In a magnetic couple, two magnets coupled together, such as shown in figure 1.1, span a gap. This allows them to transmit torque without mechanical contact with one another.

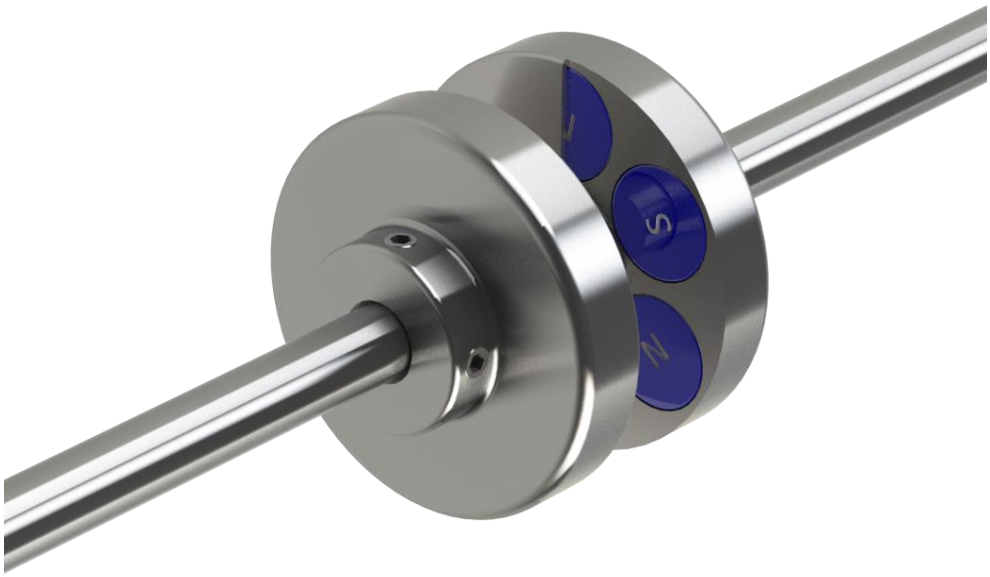

Figure 1.1. An example of a magnetic couple from TEA Machine Components Inc, Magnetic Coupling. https://www.teausa.net/Latest-News/Post/631/Magnetic-Couplings. Accessed 6 May 2019 [11].

Torque can be transmitted across a separation wall, from a primary driver to a follower, making it ideal for some applications such as a sealless fluid pump. Naval propulsion gives another example; in this case torque is transmitted between the motors and propellers (shown in figure 1.2). In the chemical industry, such drivers can prevent leakage of fluid and fugitive emissions that may be expensive, or harmful to health of the environment. This couple is also beneficial for isolated systems, such as a vacuum or high-pressure vessel.

This magnetic couple replaces the axle, that would have been otherwise used to transfer power from the motor to the load side. Using figure 1.2 as an example, the motor is still able to transfer the rotational power to rotate the propeller, even though there is a rear wall to the boat

hull in between the two. It can do so by using the magnetic couple, instead of an axle. The magnetic field can bypass the wall of the boat hull and continue its attraction between the two magnets.

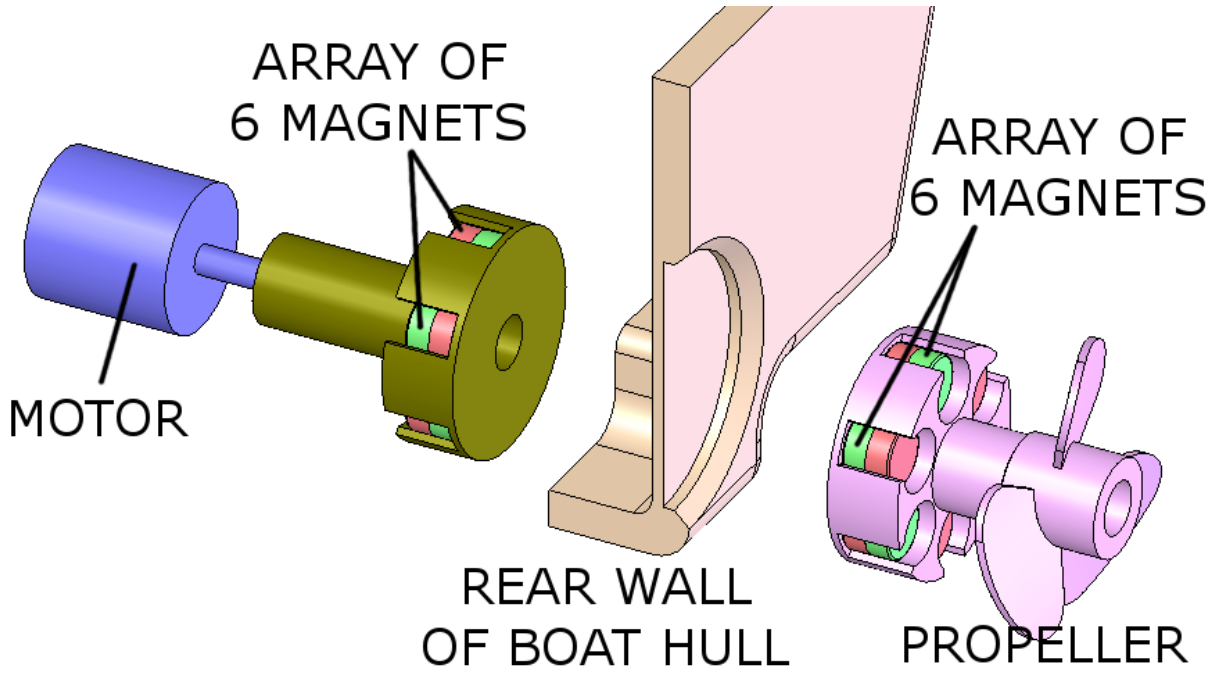

Figure 1.2. An example of a magnetic couple in a nautical setting. Image obtained from K&J Magnetics Coupling Inc, Magnetic Coupling boat. [10] https://www.kjmagnetics.com/blog.asp?p=magnetic-coupling. Accessed 6 May 2019

Typically, one component that fails first, when having a system with an axle is the O-ring that would create the seal to prevent water from leaking. The O-rings typically become brittle and bust which initiates the leak. By having a magnetic couple and eliminating the axle that

would initially go through the wall, one would also eliminate the possibility of the type of mechanical failure.

Furthermore, since a magnetic couple is modular, if a piece were to break, the piece would be more accessible to fix since one would only have to work with a part of the system instead of the whole. For example, if the propeller was to become damaged, or if the motor was to burn out, the user would be able to replace that half. As a result, it will also lower routine maintenance costs.

When constructing the couple, the two sides so not have to be precisely aligned with one another (however, it would be ideal) [3][7]. The magnetic couple may not be parallel with one another and have a slight degree off angle, or the magnetic couple may not align perfectly in front of one another, and it will still achieve power transfer.

Moreover, the couple has torque limitation in critical applications when facing a maximum transmissible torque (pull-out torque). For instance, avoiding mechanical failure by giving intrinsic overload prevention which allow the magnetic couple to increase the lifetime and efficiency of the system. Having the motor not directly attached to the propeller reduces noise, vibrations, and mechanical friction losses. There is also an advantage in the system in which a propeller or rotor on the load side could become stuck. This creates stress on the axle, that would be leading to a broken axle or overloaded motor. Since there is no contact, the couple will create slip, if one end jams. Slip is where one side will stop rotating while the other one continues. It as well eliminates the need for a more powerful motor that would initially be used to compensate the start-up torque [2][13] [16][19].

1.2 Types of Couplings

When studying various types of non-contact mechanical couplings to transfer torque, one may study one of the following: axial, coaxial and, eddy current couplings. Axial and coaxial couplings are both synchronous while the eddy-current is an induction type coupler. Both have radial and flux configuration.

1.2.1 Synchronous couplings

In synchronous couplers, shown in figures 1.1 and 1.2, both the drive and the load side of the couple rotate together. The poles are paired together and will rotate in sync. Figure 1.3 displays a 2-D model of the magnetic couple and uses arrows to illustrate the magnetic field between the magnets. The north facing magnets are red, while the south facing magnets are blue. The rotation or movement of one rotor is shown with a green arrow. The black arrows represent the magnetic field between the initial attraction of two magnets. The white arrows show the magnetic attraction between the two magnets after the slip. In figure 1.3a, the two rotors of the magnetic couple are directly in front of one another with both rotors' static. Figure 1.3b shows the bottom or drive side rotor moving to the right. The black arrows show the magnetic field still attracted to one another but slightly angled. Figure 1.3c shows the second rotor moved far enough to the right, that it is at a distance causes the magnets to align in front of the top rotor and has the magnets with the same facing polarity facing one another. The black arrows show the magnetic attraction of the first pair, while the white arrows show the magnetic attraction to the next magnet. This slipping creates a new magnetic pair. Figure 1.3c also shows the moment before the slip occurs. This moment is where the pull-out torque (maximum torque) is measured. Figure 1.3d shows the moment after the slip occurs. The magnets are then attracted to the next magnets, and the new magnetic pair is created.

This illustration demonstrates the workings of the magnetic couple on a two-dimensional plane. The illustration simulates the movement of one rotor (bottom) and the magnetic fields' reaction imposed onto the other rotor, or load side rotor. In this case, the load side rotor has a larger load than the pull-out torque, thus creating slip and not a rotation on the load rotor.

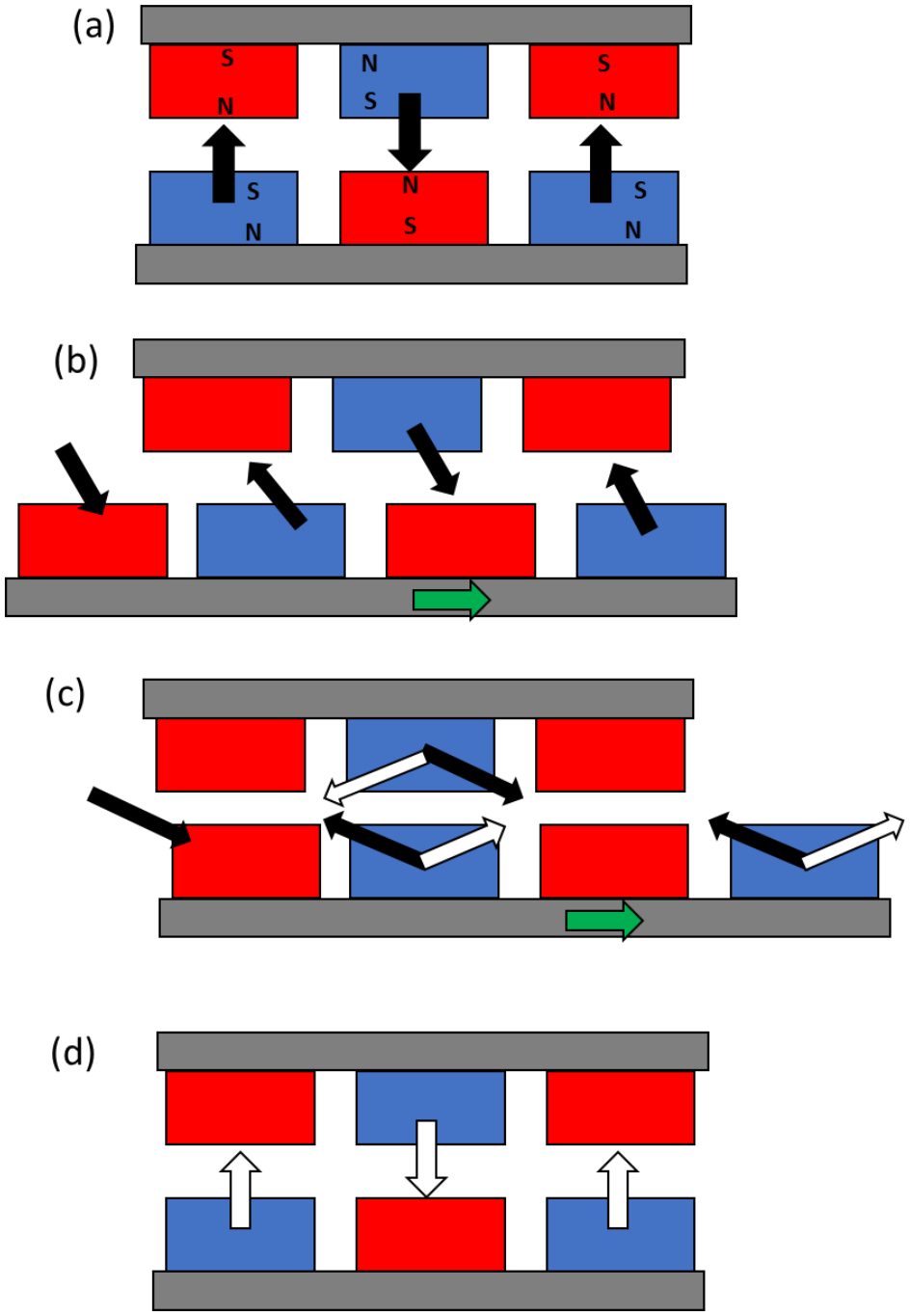

Figure 1.3. 2-D model of the axial magnetic coupling. (a) shows the couple directly in front of one another. (b) shows the bottom rotor moving to the right. (c) shows the bottom rotor continue moving to the right but not directly in front of the next magnet, at the moment right before the actual slip occurs. (d) shows the arrangement of the magnets after slip occurs.

1.2.1a Axial

An axial couple is shown in figure 1.4a consisting of two opposing identical discs or rotors, equipped with rare earth permanent magnets. The magnets are magnetized in an axial direction. When applying torque to the load side of the disc, the two discs shift by an angle, known as the load angle. With this design, the angular shift between the two discs depends on the initial torque applied. One drawback of this design is the significant value of attractive force between the two discs.

1.2.1b Coaxial

Coaxial couplers have one member rotate inside the tube, which is the second member. This type of couple is used to produce a larger torque. The transmitted torque is independent of speed and dependent only on the relative angle of displacement of the coupler halves [13]. This couple is shown in figure 1.4(b).

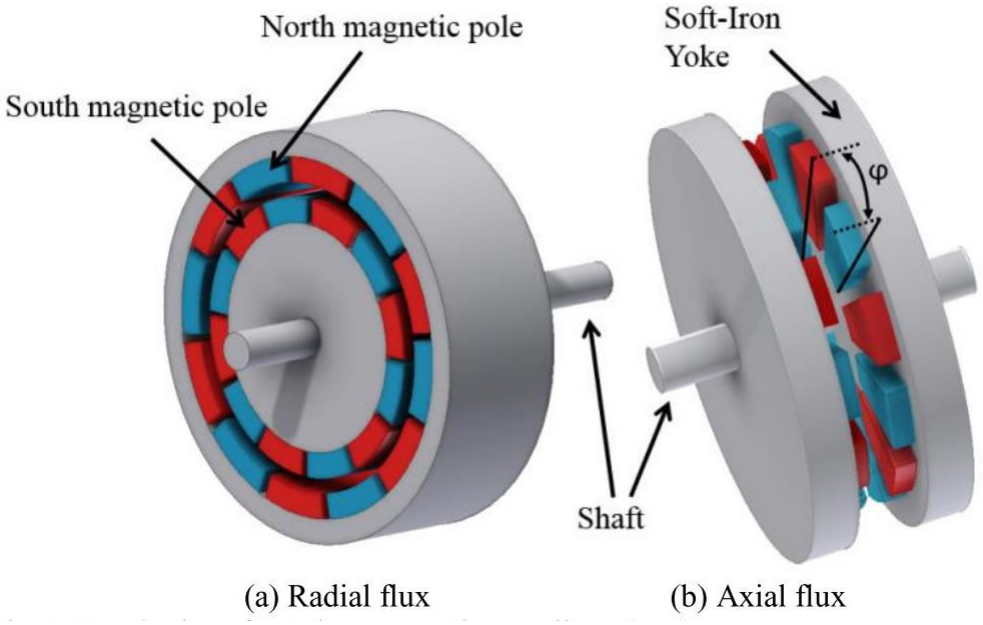

Figure 1.4. This shows the two types of synchronous magnetic couples (a) being a Radial flux magnetic couple and (b) being an Axial flux magnetic couple used from Dolisy reference [2].

1.2.2 Induction coupling

The induction couplers work from the slip created between the couple. When disc one rotates faster than the other, a current is induced to the second disc. The induction imposed onto the second disc then creates a rotation drive leading to the second disc rotating. This coupling consists of two discs shown in figure 1.5. One of the discs is composed of rare earth magnets, similar to synchronous couplings; however, the other disc is equipped with a conducting plate, such as copper. The workings of the couple are induced when the conducting plate creates slip

and interacts with the magnetic field. This generates a coupling force on the permanent magnets, hence the transmission of torque. [2][4][8][19]

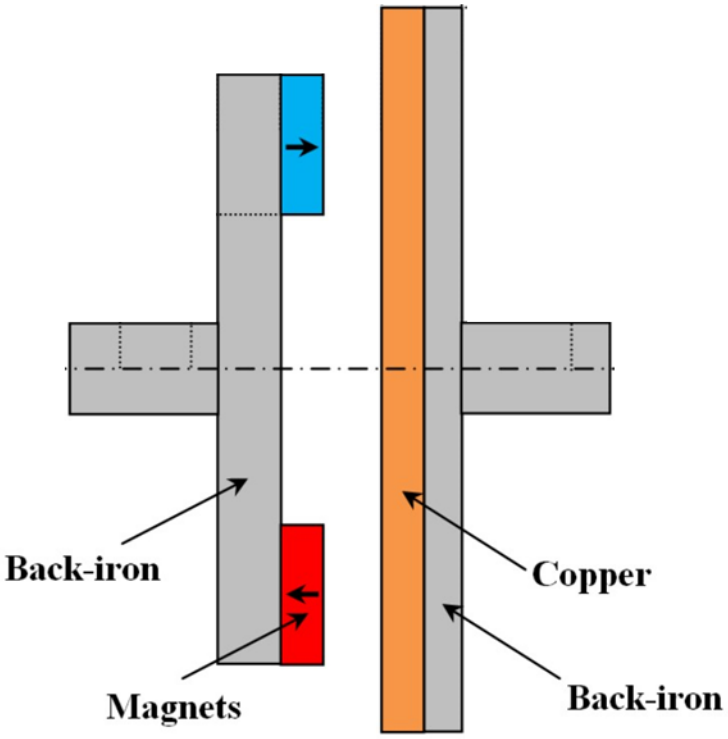

Figure 1.5. Cross section of the studied axial-flux permanent magnet eddy-current coupling adapted from Frontchastagner reference [4].

1.3 Motivation

The goal of the research was to measure and find a relationship between the pull-out torque and the air gap distance between the coupler that arises when permanent magnetic couples are approaching each other. The influence on the coupling characteristics such as the permanent magnet's geometry, the number of dipole pairs, and polarity arrangements were compared to investigate the air gap size on the magnitude of pull-out torque. The results are compared to the analytical expressions that model the magnetic fields. [2][5]

2. Theory

To better understand experimental results on the magnetic couple, prior research based on computational models and analytical calculations were examined. This discussion generally follows the approach by B. Dolisy, S. Mezani, T. Lubin, and J. Lévêque, (see reference 2), using analytical expressions to model the axial flux magnetic couple.

Analytical models can provide closed-form solutions giving focus on the results and insight they yield. These are useful tools for first evaluations of magnetic couplings performance and the first step of design optimization. The proposed model is a design for magnetic couplers with an axial magnetic flux coupling. The analytical models of magnetic couplings were developed by solving the partial differential equations that come from Maxwell's equations, but the approach of ref. [2] was adapted to the geometry of this project. The analytical method computes the torque for magnetic couplings and is based on boundary value problems with Fourier analysis. This method consists of solving Maxwell's equations in the different regions (magnets and air gap) by separation of variables method. The magnetic field distribution is obtained in each region by using boundary and interface conditions and using a magnetic scalar potential formulation. Then using the mathematical analogy between the electrostatic and the magnetostatics fields, the magnetic force acting on the magnets placed on the opposite side is obtained by using the equal electrostatic Lorentz force. The torque is then found by using Maxwell's stress tensor. The torque expression is used to study the influence of geometrical parameters (number of pole pairs and air-gap length). The analytical model created is compared with the experimental results to explore the accuracy of each. [2][6][7][8]

In the axial flux couplings design, the two discs(rotors) are created to be identical and facing one another and have an array of rare earth permanent magnets that are alternately magnetized along the θ-direction. For our base model used within the derivation of the analytical model, the magnetic couple uses the same number of pole pairs. (p=6 in Figure 2.1).

Figure 2.1 shows the arrangement that was used for the analytical model. It also shows variables: r, r_{mc}, D_x, and D_y, with values explained in table 2.1. A synchronous magnetic couple transmits torque across a drive system. This is typically done by having a drive side (presumably connected to a motor) and a load side move in sync with one another through a magnetic couple that replaces an axle that otherwise would have connected the two sides together. By doing this, the magnetic couple would need to have a magnetic flux density that is greater than the pull-out torque. The pull-out torque is the maximum torque the system would allow before it creates slip and an abrupt drop in speed. The analytical model is used in comparison with the experimental model to create an empirical equation that can lead to model future drive power in magnetic couples.

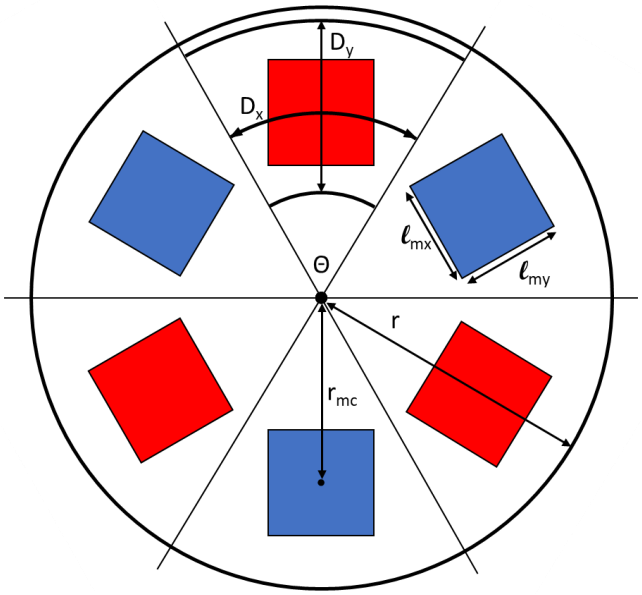

Figure 2.1. The geometry of the axial-type magnetic coupling that has six dipole pairs (p=6)

Table 2.1. Values and descriptions for the dimensions of the magnetic couple components.

Parameter	Description	Unit	Value
l_{my}	Length of the magnet in the y-direction	mm	25.4
l_{mx}	Length of the magnet in the x-direction	mm	25.4
D_x	Length of the Domain along x	mm	46.5
D_y	Length of the Domain along x	mm	50.8
r	Radius of the disc	mm	69.8
r_{mc}	Radius to the center of the magnet	mm	44.4
Θ	Arclength degree	degrees	60°
v	Thickness of air gap	mm	Variable
α	Magnet to pole opening ratio	-	.55
p	Number of pole pairs	-	Variable (but determined before each experiment, this case uses 6)
B_r	Residual induction of permanent magnets	T	1.32

2.1 Magnetic force from the Electrostatic-Magnetostatics analogy

In Maxwell's formulation, electrostatics have parallel interactions while magnetism operates ninety degrees apart. This is because electromagnetism interacts perpendicularly to each other. However, in a system, such as this couple, in which only magnetism exists, it is possible to

define magnetism in a parallel fashion. This approach makes solving forces a matter of solving boundary conditions and similar to a number of common approaches found in electrostatics. The expression will be derived using the analogy between the electrostatic and the magnetostatics fields, to find our pull-out torque value. To begin this, one would need to consider being in free space. Being in free space allows an electrostatic uniform surface charge density σ_S (C/m2) to be subjected to an electric field $\vec{E}$. The Lorentz force (N) exerted on σ_S is

$$\vec{F}_S = \sigma_S \iint_S \vec{E}\, dS \tag{1}$$

where S is the surface which carries σ_S.

From the magnetostatics perspective, one may consider using an equivalent magnetic surface charge σ_m(A/m). For modelling purposes, the magnetic charge (σ_m) is introduced to replace some magnetic field sources. Using the analogy stated previously between the magnetostatics and the electrostatic force, given by (1), the magnetic force (N) is then obtained by

$$\overrightarrow{F_S} = \sigma_m \iint_S \vec{B}\, dS \tag{2}$$

Here, S is the surface which carries σ_m.

The force expressions (1) and (2) show that the electrostatic-magnetostatics analogy connects the electric field $\vec{E}$ to the $\vec{B}$ field (called flux density).

Relating this to the magnetic coupler, one needs to compute the force through the magnet's magnetic surface charge on one disc and the magnetic field created by the magnets of the second disc. Expression (2) uses Lorentz force in free space provides the correct values of the force along the x and y directions for the coupler. However, magnets give a force in the z-direction, so (2) will not give the true value of the force, and the Maxwell stress tensor incorporated.

2.2 Magnetic field due to the magnets of one rotor

The magnetic field is assumed null in the housing for two reasons: there are no added components that give off a large enough magnetic field, and for simplicity. The boundary condition on housing is

$$\vec{n} \times \vec{H} = 0 \tag{3}$$

where $\vec{n}$ is the outward direction normal to the considered surface and $\vec{H}$ is the magnetic field strength. Rare-earth permanent magnets have a relative permeability close to that of air (μ_r = 1). It is then more convenient to use a magnetic scalar potential (Φ) formulation ($\vec{H} = -\nabla \Phi$) to solve the magnetostatic problem. The flux density $\vec{B}$ is given by

Air region: $$\vec{B} = -\mu_0 \nabla \Phi \quad (4)$$

Magnets region: $$\vec{B} = -\mu_0 (\nabla \Phi + \vec{M}) \quad (5)$$

where $\vec{M}$ is the magnetization of the magnet.

D_x is found at the magnets center and uses the arc length that equally spaces the magnets apart from one another. This allows for the problem to be solved in a Cartesian coordinates system. Figure 2.2 shows the main dimensions of the linearized coupler in a 3-dimensional space. The dimensions of the magnet are l_{mx}(the length of the magnet in the x direction), l_{my}(the length of the magnet in the y direction) and h (thickness of the magnet along the z-direction). D_x (Domain in the x-direction) is found by calculating the arclength around each individual magnet, by using the radius to the magnets center and theta, equaling the 360° divided by the number of dipole pairs(p). Since the model assumes an alternating polarity relationship, only one pole is considered with anti-periodic boundary conditions along both the x and y axis [2]. D_y (Domains of the magnet in the y-direction) is fictitious but needed to get a solution [2]. By setting $D_y >> l_{my}$, gives a realistic solution and for best results $D_y = 2l_{my}$. The airgap between the two rotors is noted as *v*.

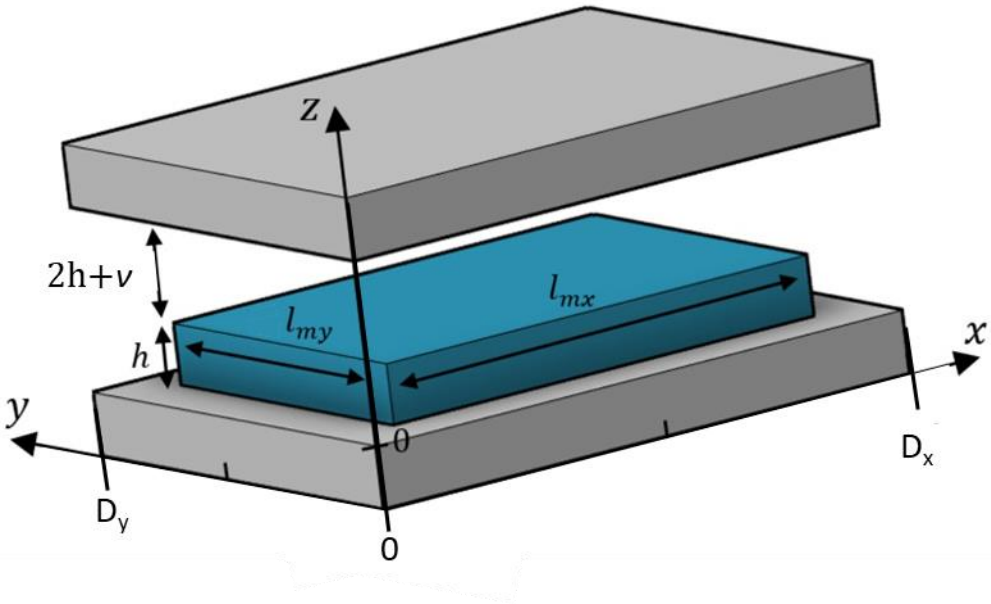

Figure 2.2. 3-D image of the dimensions of one magnet pole after linearization adapted from Dolisy from reference [2] fig.3.

Domain I ($0 \leq z \leq$ h) is composed of the region of the magnet along the z-axis. The magnetization vector is noted $\vec{M}= M_z(x,y)\ \vec{e}_z$. The boundary conditions require that magnetism reaches zero at the top and bottom of the magnet. The solution is thus obtained by expanding the magnetization into a double Fourier series along x and y-directions as shown in figure 2.5.

$$M_z(x,y) = \sum_{n=1}^{\infty} \sum_{m=1}^{\infty} M_{n,m}\, cos(w_n x)\, cos(w_m y) \tag{6}$$

$$\text{with } M_{n,m} = \frac{16B_r}{u_0 nm\pi^2} \sin(w_n l_{mx}) \sin(w_n l_{my})$$

$$w_n = \frac{n\pi}{D_x}; \omega_m = \frac{m\pi}{D_y}$$

where *n*, *m* are odd integers, and B_r is the residual flux density of the permanent magnets measured in Tesla. The magnetization given by (6) is divergence free $\nabla \cdot \vec{M} = 0$.

Domain II ($h \leq z \leq h_t$) corresponds to the actual air-gap and the second magnet (whose magnetization is turned off). The magnetic scalar potential is noted Φ_I in domain I and Φ_{II} in domain II are shown in the following expression (7) respectively. Φ_I and Φ_{II} are the solution of Laplace equation[2]

$$\nabla^2 \Phi_I = \nabla \cdot \vec{M} = 0 \tag{7}$$

$$\nabla^2 \Phi_{II} = 0$$

Figure 2.3 shows the x,z plane of one magnet, and shows each domain and the magnetization. This figure also shows the dimensions along the z-axis, where the entire region (domain I and II) consists of both magnets and the air gap between, noted as h_t, where h_t= 2h+v.

Figure 2.4 shows the magnetization as a function of x and y. It also gives a better comparison of each of the domains.

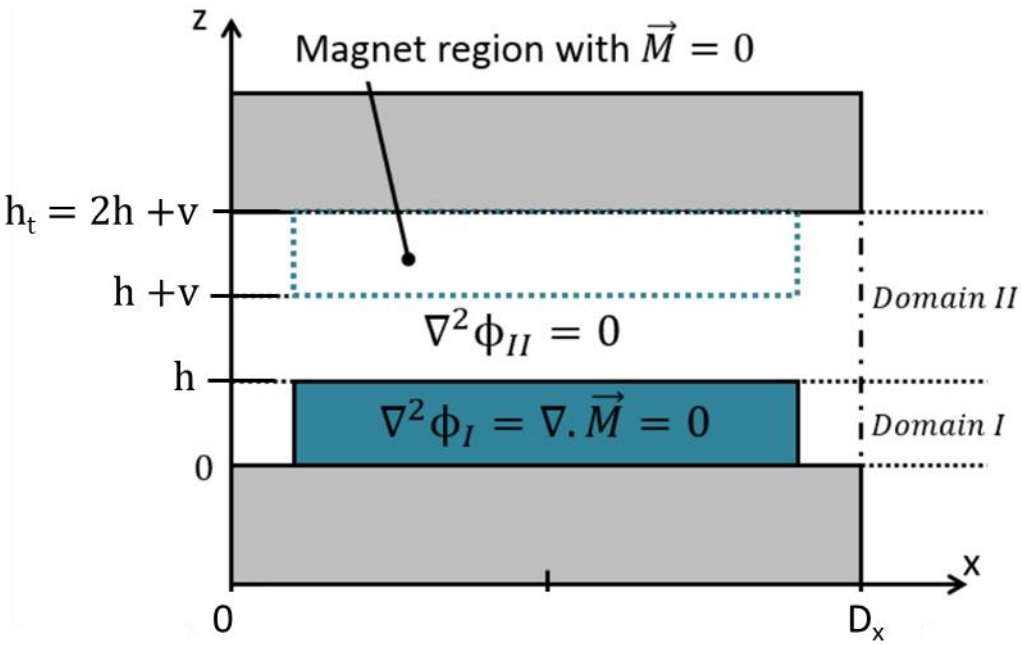

Figure 2.3 Domains and equations in the plane (x,z) adapted from reference [2] fig 4.

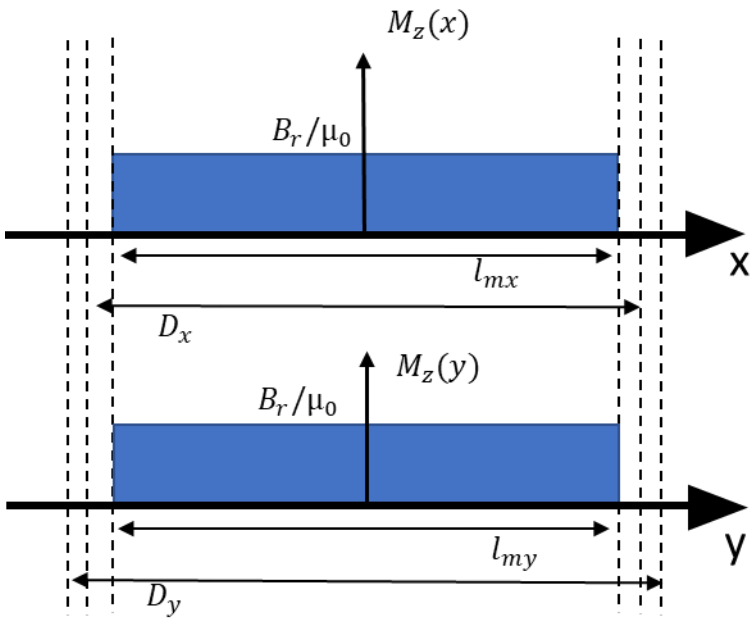

Figure 2.4 shows the magnetization M_z as a function of x and y (domain I)

By considering the anti-periodic boundary conditions along with the x and y coordinates, the use of the method of separation of variables provides the following form solutions for Φ_I and Φ_{II}

$$\Phi_I(x,y,z) = \sum_{n=1}^{\infty}\sum_{m=1}^{\infty}\left(A_I e^{kz} + B_I e^{-kz}\right) \times cos(\omega_n x)\, cos(\omega_m y)$$

$$\Phi_{II}(x,y,z) = \sum_{n=1}^{\infty}\sum_{m=1}^{\infty}(A_{II} e^{kz} + B_{II} \mathrm{e}^{-kz}) \times \cos(\omega_n x)\cos(\omega_m y) \tag{8}$$

$$\text{With } k = \sqrt{w_n^2 + w_m^2}$$

The coefficients A_I, B_I, A_{II} and B_{II} are obtained using the interface and boundary conditions[2]. The boundary condition in domains I and II are set at z=0 and z=h_t, respectively. These conditions state that the tangential magnetic field components H_x and H_y are zero. This leads to

$$A_I + B_I = 0 \tag{9}$$

$$A_{II} e^{kh_t} + B_{II} e^{kh_t} = 0$$

Interface conditions between domains I and II are set at z=h. Domain I and II have the same magnetic permeability (μ_r=1), so the normal flux density (B_r) and the tangential magnetic fields (H_x and H_y) of the domain I and II will be equal at z=h. The two following expressions arise

$$A_I e^{kh} + B_I e^{-kh} - A_{II} e^{kh} - B_{II} e^{-kh} = 0 \tag{10}$$

$$A_I e^{kh} - B_I e^{-kh} - A_{II} e^{kh} - B_{II} e^{-kh} = \frac{M_{n,m}}{k}$$

The coefficients A_I, B_I, A_{II}, and B_{II} are calculated by solving an algebraic system of linear equations from (9) and (10) given by,

$$A_I = -B_I = \frac{M_{n,m}(e^{2kh} - e^{2kh_t})}{2ke^{kh}(e^{2kh_t} - 1)}$$

$$A_{II} = -\frac{M_{n,m}\, sinh(hk)\, e^{-kh_t})}{2k \sinh(h_t k)} \tag{11}$$

$$B_{II} = \frac{M_{n,m}\, sinh(hk)\, e^{kh_t})}{2k \sinh(h_t k)}$$

2.3 Equivalent surface charge density of the second PM rotor

The surface charge density of a magnet with uniform magnetization is given by

$$\sigma_m = \vec{M} \cdot \vec{n} \tag{12}$$

Where $\vec{M} = M\vec{e}_z = B_r/\mu_0\vec{e}_z$ is the magnetization vector while $\vec{n}$ represents the outward normal to the respective surface. This dot product is to be performed on all the external surfaces of the magnet volume.

Figure 2.5 shows a rectangular permanent magnet with a uniform magnetization in the z-direction. The magnet is represented by two surface charge densities: σ_+ and σ_- (from expression (12)). The surface charge density $\sigma_+ = M$ is located at $z = h_t$ and the surface charge density $\sigma- = -M$ at $z = h + e$.

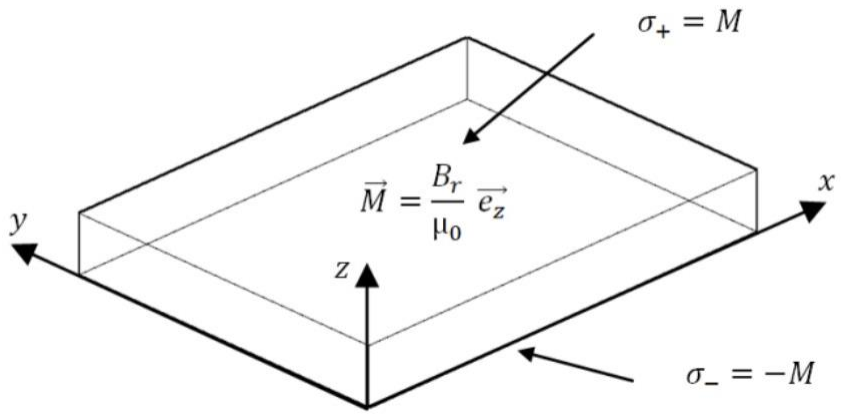

Figure 2.5 Equivalent surface charge density for a rectangular permanent magnet used from Dolisy reference [2] fig 6.

2.4 Torque expression

The force is computed using expression (2) where integration is performed on the surfaces carrying σ_+ and σ_-. However, according to the boundary condition from expression (3), the components B_x and B_y of the flux density are null on the charged surface σ_+ (at $z = h_t$), so the forces that contribute to torque (F_x and F_y) are also negligable. Hence, the integration is only performed on the charged surface σ_- (at $z = h + e$).

The axis of rotation (the shaft axis) is parallel to the 0 in the z-axis. This axis has constant coordinates noted (x_0,y_0) in the reference frame. The z-component of the torque is then obtained by

$$T = \int_{-l_{mx}+X_i}^{l_{mx}+X_i} \int_{-l_{my}}^{l_{my}} \left[(x - x_0)f_y - (y - y_0)f_x\right]dxdy \tag{13}$$

The variable X_i in the limits of integration in equation (13) corresponds to the angular lag (load angle) φ between the two rotors of the coupling. X_i and φ are related by $\varphi = X_i/r_{mc}$ where r_{mc} is the radius to the magnets center. Notice that the maximum (pull-out) torque is obtained for a position $X_i = D_x$. In (13), f_x and f_y represent the force densities in (N/m²) obtained by replacing the flux density expression (4) in the force expression (2).

$$f_x = -\mu_0 \sigma_- \left. \frac{\partial \Phi_{II}(x,y,z)}{\partial x} \right|_{z=h+e}$$
$$f_y = -\mu_0 \sigma_- \left. \frac{\partial \Phi_{II}(x,y,z)}{\partial y} \right|_{z=h+e} \quad (14)$$

The force density f_y, being symmetrical along the y-direction, corresponds to the torque obtained by integration between along l_{my} and disappears. Hence, for 2ρ poles, and $y_0 = -r_{mc}$ the torque expression (14) becomes

$$T = \int_{-l_{mx}+X_i}^{l_{mx}+X_i} \int_{-l_{my}}^{l_{my}} (y + R_{mc}) \left. \frac{\partial \Phi_{II}}{\partial x} \right|_{z=h+e} dxdy \quad (15)$$

Finally, from (8) and (11) an analytical expression for the torque is obtained after integration of (15)

$$T = \sum_{n=1}^{N} \sum_{m=1}^{v} \frac{128\, p\, B_r\, R_{mean}}{\pi^2 \mu_0\, n\, m\, k\, w_m} sin^2\left(\alpha\, n\, \frac{\pi}{2}\right) sin^2\left(\omega_n\, l_{m_y}\right) \frac{sinh^2(k\, h)}{sinh(k\, h_t)} sin(n\, p\, \varphi) \quad (16)$$

Where n and m are the number of harmonic terms used for the torque calculation.

Within this entire expression, the most important relation for this experiment is $\frac{1}{sinh(k\ h_t)}$. Since my measurements vary the air gap distance, ν, is within the parameter of $sinh(k\ h_t)$, where $h_t = 2h + \nu$, this parameter will be examined further. The hyperbole sine

$$sinh(k\ h_t) = \frac{e^{k(2h+\nu)} - e^{-k(2h+\nu)}}{2} \approx \frac{e^{k(2h+\nu)}}{2} \tag{17}$$

Considering this hyperbolic sine is in the denominator this provides

$$T \propto \sum e^{-K(2h+\nu)} \tag{18}$$

3. Experimental Methods

For the construction of the axial magnetic couple, many components were used to solve a variety of design problems that occurred. Initially, there was a need for the magnets to be secured onto each disc, and for those discs to move freely from one another. First, a disc housing was created for the magnets to be placed in. This housing is shown in figure 3.1. An aluminum disc was used to connect the disc to the axle through a ceramic ball bearing. This allowed the disc to become a rotor and move freely. An acrylic disc was created to restrict the movement of the magnets in the x and y-direction. Between the acrylic and aluminum backing, a disc of a steel sheet metal was placed. The sheet metal completed the magnetic circuit of the magnets as well as prevented the magnets from moving in the z-direction. An acrylic disc was placed over the magnets to secure everything together.

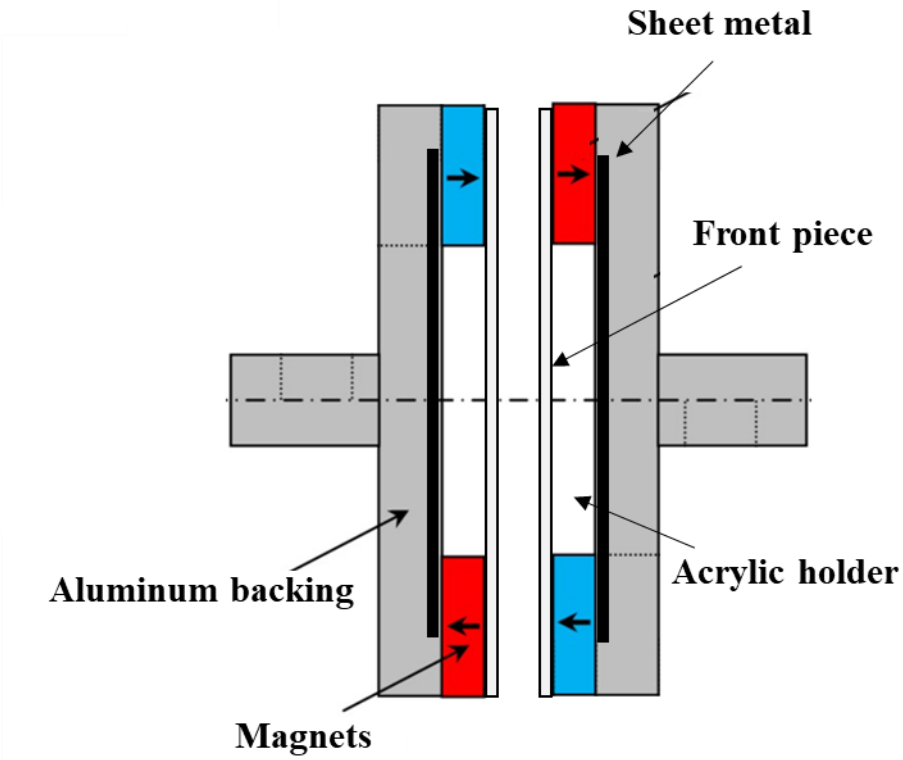

Figure 3.1. Transverse view of the created magnetic coupler showing the axles, aluminum backing, steel sheet metal, magnets, acrylic holder, and the front piece

3.1 Design

The design of the face-to-face magnetic couple consisted of many layers. The initial design for the first experiment was to create a 5.5” housing to best fit six of the 1”x 1” x 0.5” (LxWxH) magnets.

The first piece was a 0.55” thick clear acrylic sheet that was cut to 5.5”, as shown in figure 2.2c. This design was chosen to have each magnet equally spaced around the acrylic

wheel, and provide 0.25” space from the magnets and the edge. The 0.25” thickness was chosen because this gave the structure durability in case the acrylic was ever dropped. Each acrylic was milled to the exact dimensions of the magnets.

The next piece created was the steel metal sheet, figure 3.2(b). This sheet was used to complete the magnetic circuit. The metal sheet also provided stability to the housing and prevented the magnets from moving in the z-direction as previously stated.

The next piece created was the aluminum backing, figure 3.2(a). To ensure that there would not be any added magnetic field to our housing unit, aluminum (3/16” thick) was used. The aluminum backing was also used to screw all the magnets and layered housing materials together, leaving everything compact and together.

The final piece created for the housing was the acetate plastic cover, figure 3.2(d). This cover can be optional in the experiment. If the magnets used in future experiments have a screw hole in them, then they can be screwed onto the aluminum backing. An acetate cover was used to create a sleek finish and enclose the magnets inside. The 1/8” thickness of acetate was selected to allow the use of a beveled screw to secure all the pieces together.

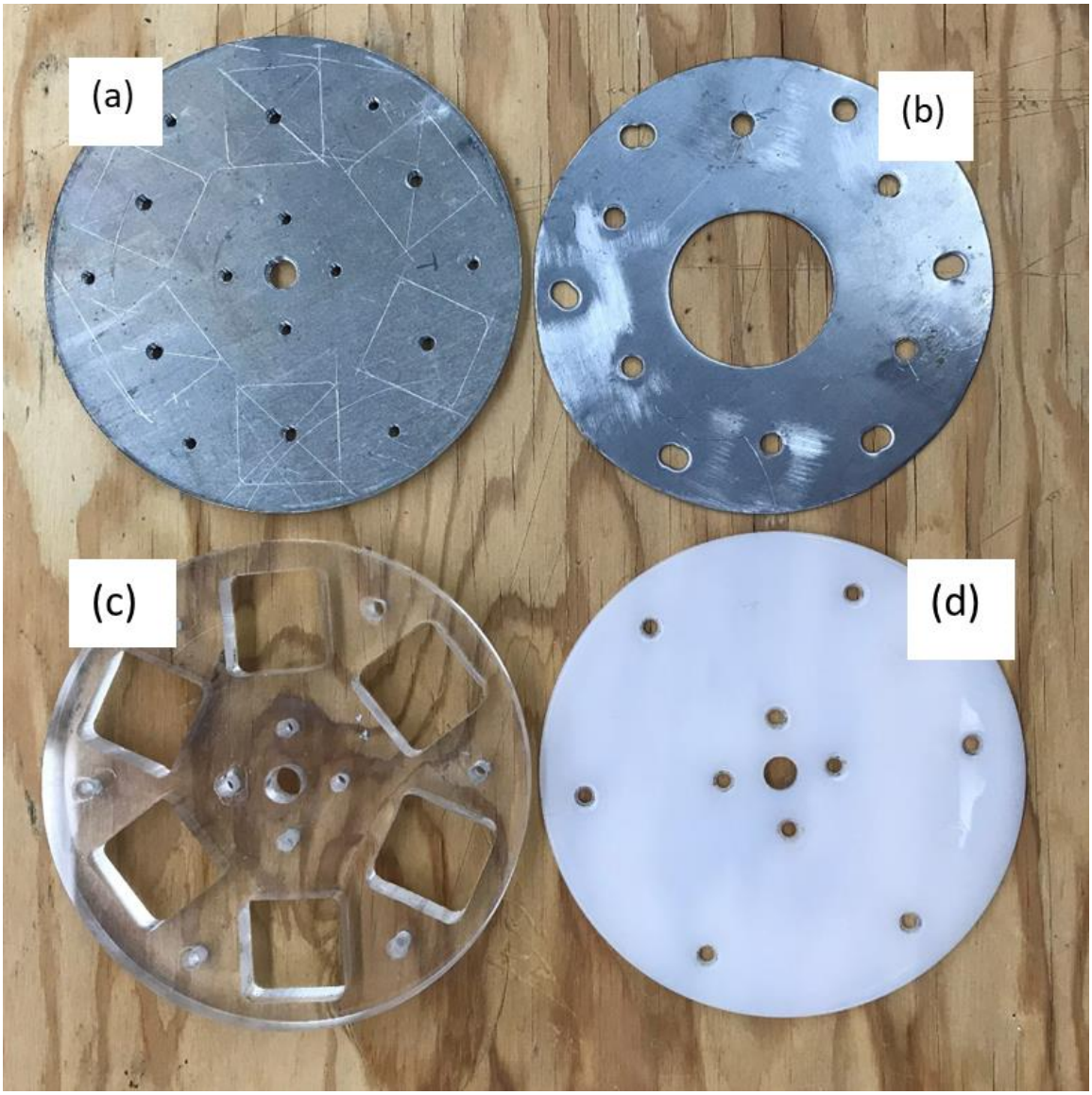

Figure 3.2. Picture of mechanical components for the housing unit. The components are a) aluminum housing back, b) sheet metal, c) acrylic magnet holder, d) front piece.

3.2 Arrangements

This section will describe all the design variations built and used for testing. In the end, there were five pairs of housing units created for the experiment shown in figure 3.3. Each arrangement was explicitly created for each test.

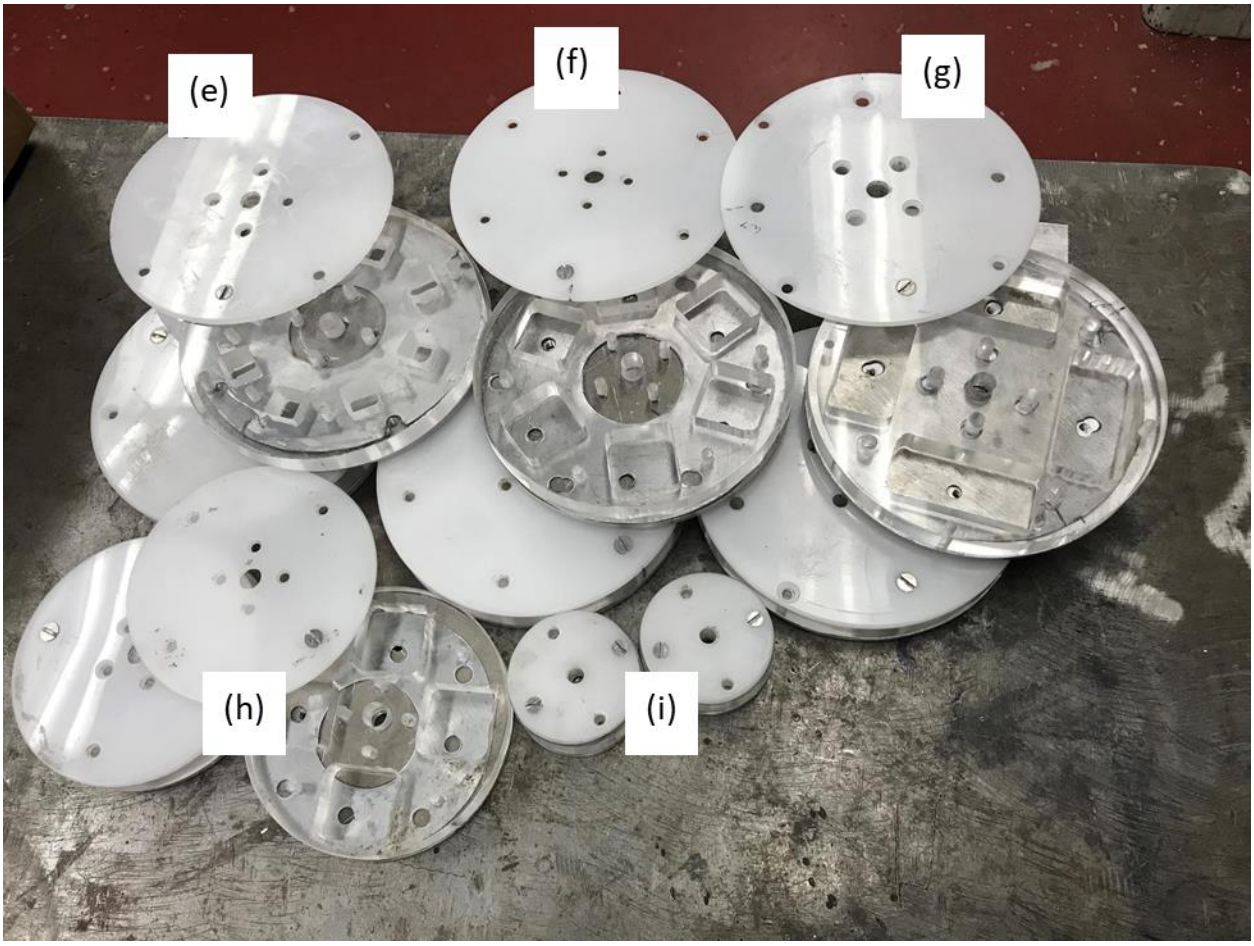

Figure 3.3. A picture of all the different housing units created for this experiment, the labels will be explained in a further section

3.2.1 Polarity Arrangements

The first experiments were to test whether an alternating arrangement rather than the same polarity arrangement would be best. In figure 3.4, two examples of an anterior view display how the magnets would be arranged in the housing unit. The blue color represents the South polarity in the front, while the red displays the North polarity in the front. This arrangement was tested with a 5.5" diameter disc that held four 2-inch rectangular magnets, six 1-inch squares, and eight 0.5" square magnets. These discs are labeled e, f, and g respectively in figure 3.3.

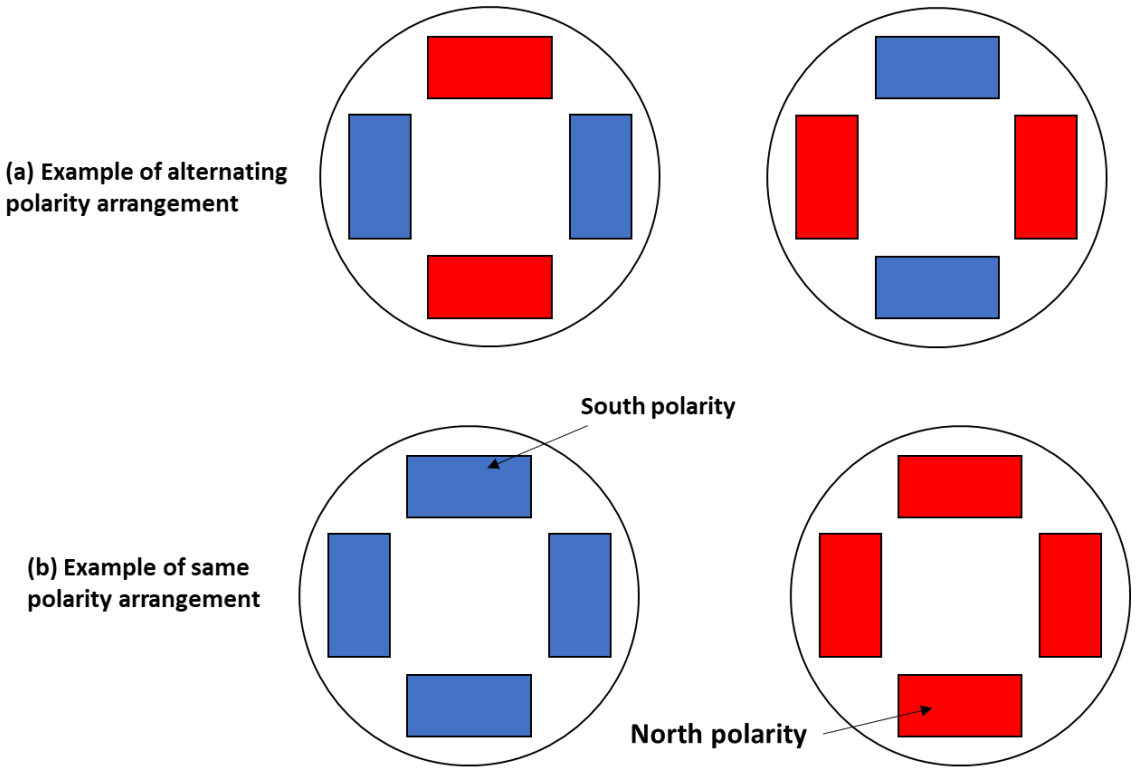

Figure 3.4. Anterior view of a magnetic couple arrangement with (a) alternating polarity and (b) homogenous arrangement. In both (a) and (b) the blue represents south facing magnets while the red squares represent north facing magnets.

3.2.2 Magnetic Strength

The first test conducted was to test how varying strengths of magnets would affect the torque. This test was constructed with four magnets on a 5.5” disc. The discs used are shown in figure 3.3(e)(g).

Table 3.1. Specifications for each magnet in this setup

Housing type from figure 2.2	Magnets used	Grade	Pulling force
(g)	Rectangle 2”x1”x0.5”	N50	87lbs
(g)	Square 1”x1”x0.5”	N55	55lbs
(g)	Round 1”d x 0.5”	ND 60	49lbs
(e)	Square 0.5”x0.5”0.5”	N52	34lbs

3.2.3 Number of Magnets

The one-inch magnets were used to test how the number of magnets would affect the torque. Figure 3.3g shows the disc that was used for the test of four magnets. Figure 3.3f shows the disc that housed the 6 magnets. Moreover, another housing unit was created that held eight 1-inch sized magnets.

3.2.5 Varying radial distances

In this experiment, the radial distance to the magnet’s center was varied. To do this, the discs were scaled down. The ratio was maintained between the radius to the magnet's center and the radius to the load. Figure 3.5 illustrates an example of the radial arm to the center of the magnet and the radial arm to the load. In this experiment they are proportionally the same

through varying test. Figure 3.3g and figure 3.3h displays the used discs. The 2” rectangle magnets were used in comparison to the 1” square magnets.

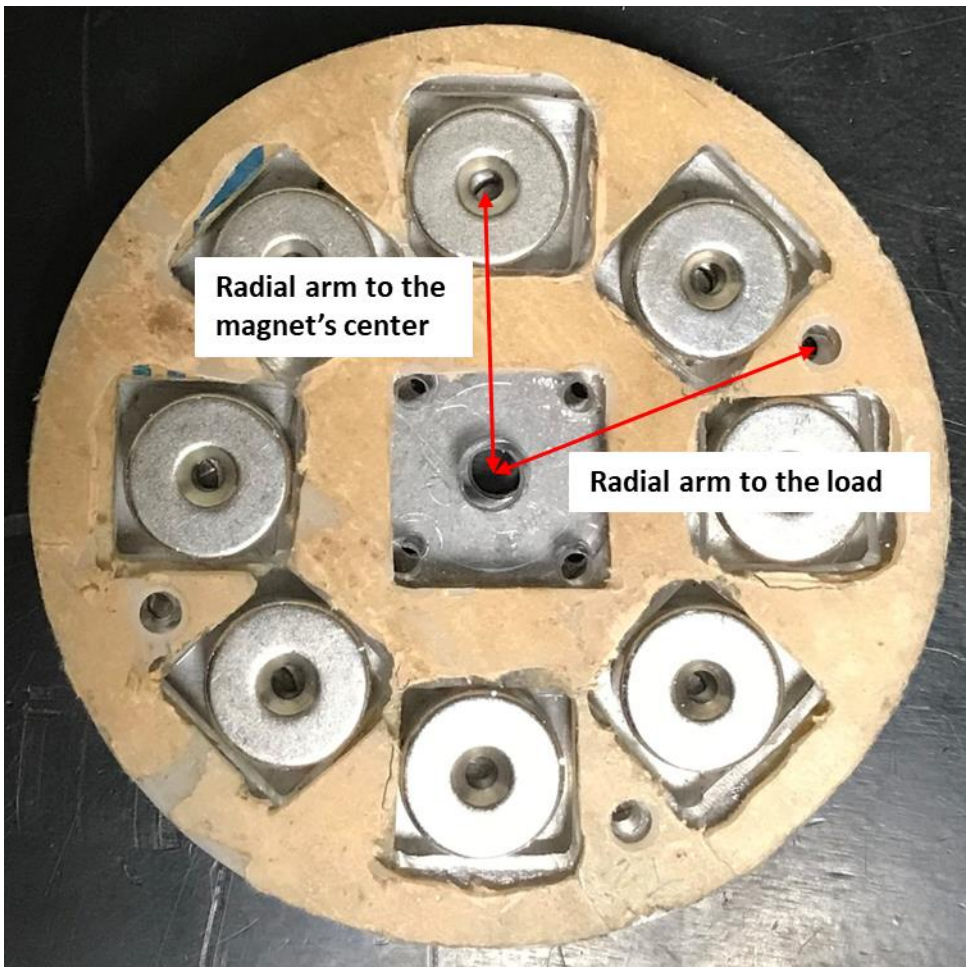

Figure 3.5. Front view of the housing unit without the cover, showing the radial arm to the center of the magnet and the radial arm to the load.

3.3 Tests

To test all the arrangements of magnets, axles are created to hold the discs and ensure they are parallel and level to one another. The axles are machined out of aluminum to eliminate any added magnetic field. The axles are screwed onto the discs and have two ceramic ball bearings to allow a free range of rotational movement. The ball bearings are surrounded with an aluminum tube that was used to secure the axle onto a stable surface. (Refer back to figure 3.1 for a transverse view of the magnetic couple).

To test the magnetic coupler, the load side is secured onto a steel table with a vise clamp. The idea behind securing it to the table was the need for an object that it is heavy enough not to allow itself to be pulled by the attraction of the magnets. The load (in grams) is added to the load side. This setup is shown in figure 3.6. The drive side of the couple had its axle attached to the bed of an upright milling machine that is secured to the ground. This allows for the drive side to be secure, but also provides the control of the bed of the mill and manipulate is manually to maneuver the drive side into place using the three-axis gear system on the mill machine. This creates a convenience when aligning the couple parallel to one another.

To find this maximum torque (pull-out torque), weights are hung from the load side of the magnetic couple. The drive side is rotates manually to see if the weights will lift or if the drive will slip. This experimentally measures the maximum torque of the magnetic couple. The experiment is repeated for varying distances. To do so, the drive side of the magnetic couple is manipulated to find the maximum air gap between the two magnetic couples at which the drive did not slip. At a given distance, the drive side would be rotated. If the load side would be unable to rotate with the drive side and slip occurs, then the distance of the air gap would

decrease, and the test will be repeated. If the load side was able to easily rotate with the drive side, then the distance of the air gap would be increased. This procedure would continue until the maximum distance between the plate that did not allow slip to occur was found (refer back to figure 1.3c for a 2-D diagram of this moment). The milling machine's digital readout system provided the distance between the two magnetic plates. The milling machine provides a resolution of <0.005" ~0.2mm.

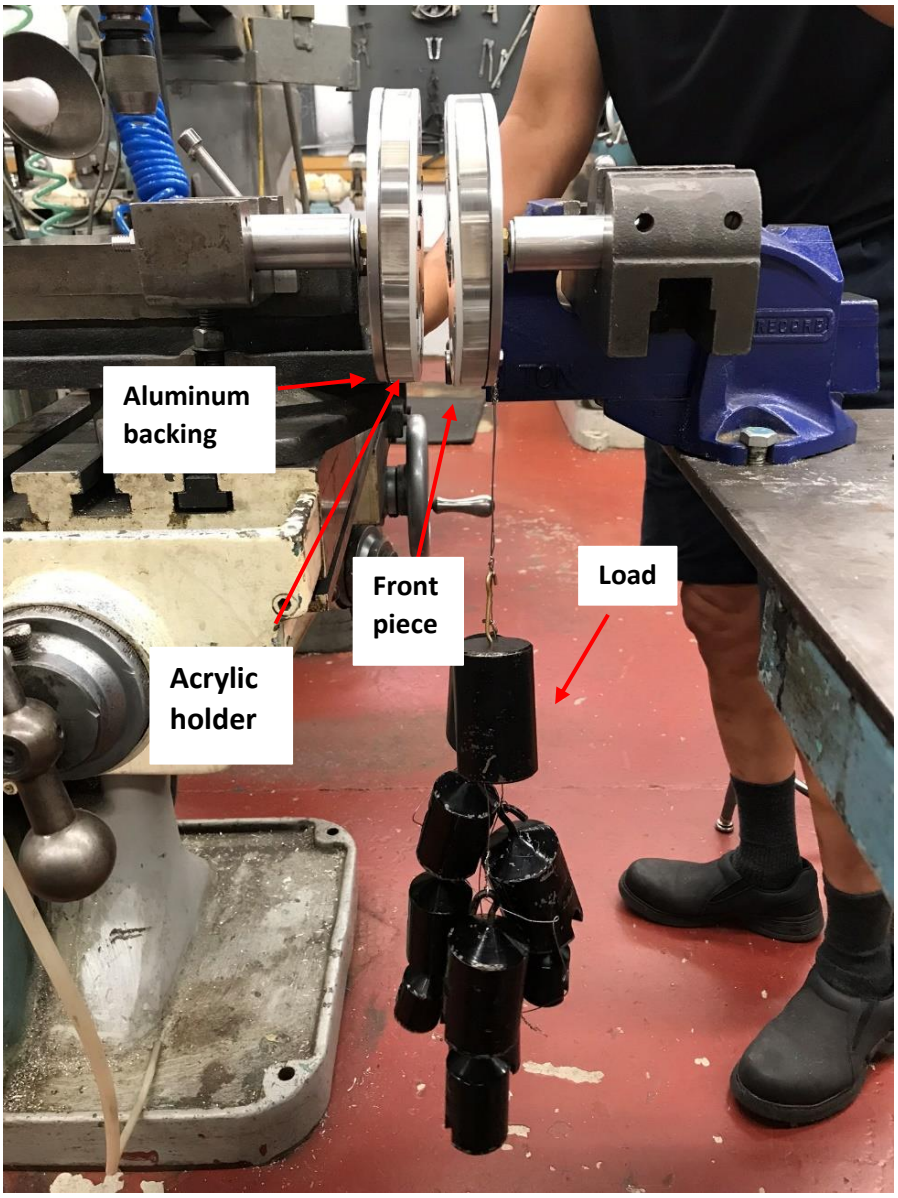

Figure 3.6. Image of data collection for torque for each magnetic arrangement with weight added to the right disc and the left disc is rotated until the couple slips.

4. Results and Analysis

To understand the nature of magnetic couples, several tests were performed with comparison to one another. The tests conducted were testing the polarity arrangements of the magnets, the strength of the magnets, the number of magnets and the radial distance that the magnets were placed. Through all the experiments, we measured the maximum weight (in grams) the load rotor was able to hold. From this, we were able to find our maximum pull out torque. Through the various arrangements we tested, we then were able to compare different ways the magnets affect the maximum torque.

4.1 Polarity arrangements

The first experiments were to test whether an alternating arrangement rather than the same polarity arrangement would be best (figure 3.4). Since our theory assumes the magnets are arranged in an alternating arrangement, we wanted to verify that this was better than the same polarity arrangement. In each graph, the blue line represents an alternating relationship while the orange line represents the same polarity relationship, and in graphs d-f the y-axis is on a logarithmic scale. Graphs (a), (b), and (c) are the raw data comparison of airgap vs the pull out torque, and are the same graphs (d), (e), and (f) respectively. Figure 4.1a shows the relationship between distance and the pull-out torque on a magnetic couple that held four 2”x1”x.5” rectangle magnets. The graph 4.1b shows the relationship between distance and pull-out torque for six 1”x1”x0.5” square magnets. The graph 4.1c shows the relationship between the distance and pull-out torque for eight 0.5” (0.5”x0.5”x0.5”) cubed magnets. In each, quantitatively a maximum torque for alternating polarity is higher than the same polarity.

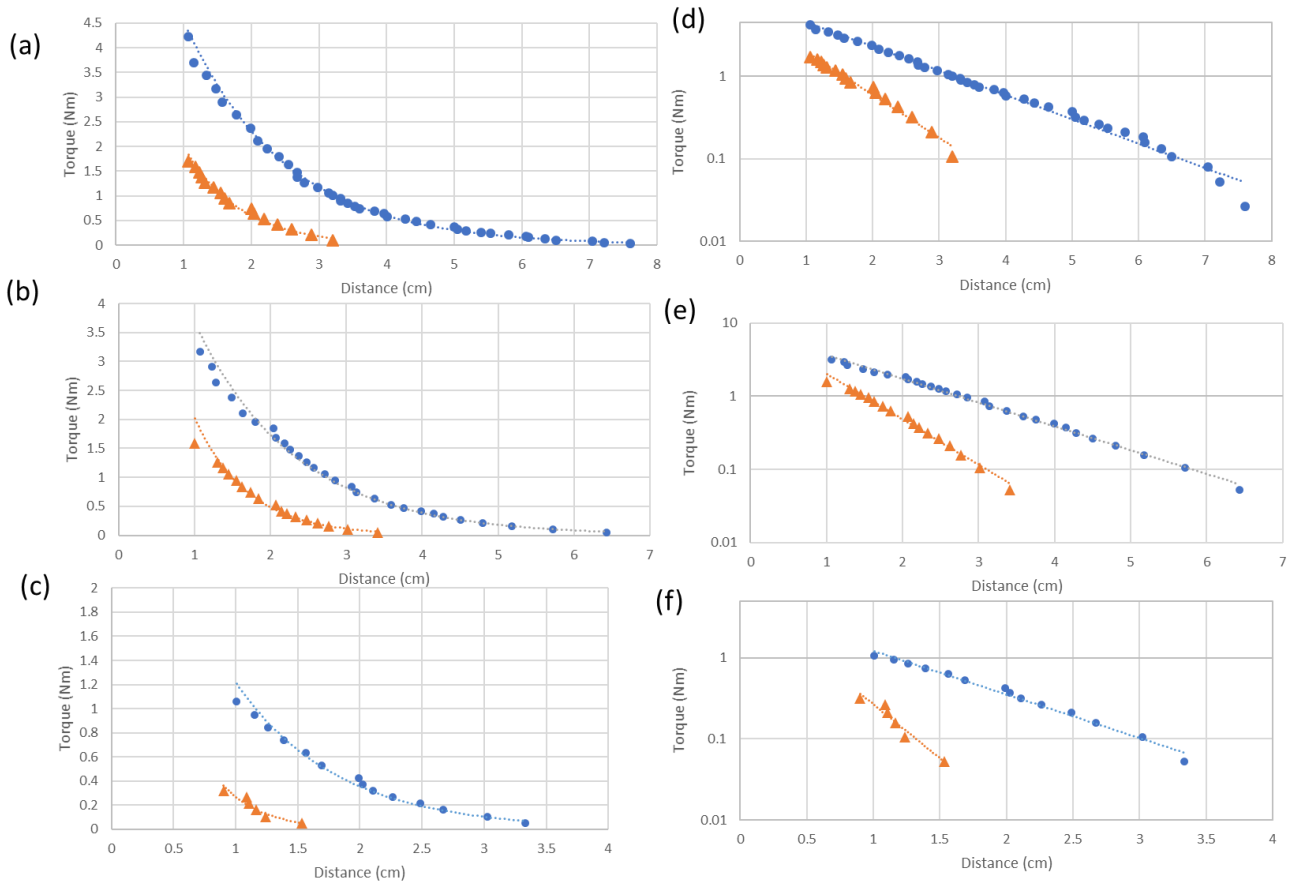

Figure 4.1. Experimental results for an alternating magnetic polarity arrangement (blue circles) vs. the same polarity relationship (orange triangles). Graphs (a), (b), and (c), are the same test as graphs (d), (e), and (f) respectively but graphs (d-f) have the y-axis on a logarithmic scale. (a) comparison of the 2" rectangle magnets (b) data collected from the 1" sq magnets (c) data collected from the 0.5" cubed magnets.

These results clearly show that an alternating polarity arrangement will provide more strength than the same polarity relationship, we then only used that arrangement for future relationships. As well, it was consistently noticed that the results are fit well by an exponentially decaying function,

$$T \propto \sum e^{-K(2h+v)} \tag{19}$$

This will be further explored in later sections.

4.2 Strength of Magnets

Next, we wanted to see how the relationship was affected by the strength of magnetic pairs. We used the 5.5" diameter disc and only used four magnetic pairs at a time. In figure 4.3, the blue (circles) line shows the 2"x1" x0.5" rectangle magnets. The orange (triangles) line shows the 1sq in x 0.5" square magnet. The grey (squares) line shows the 1" diameter disc magnet.

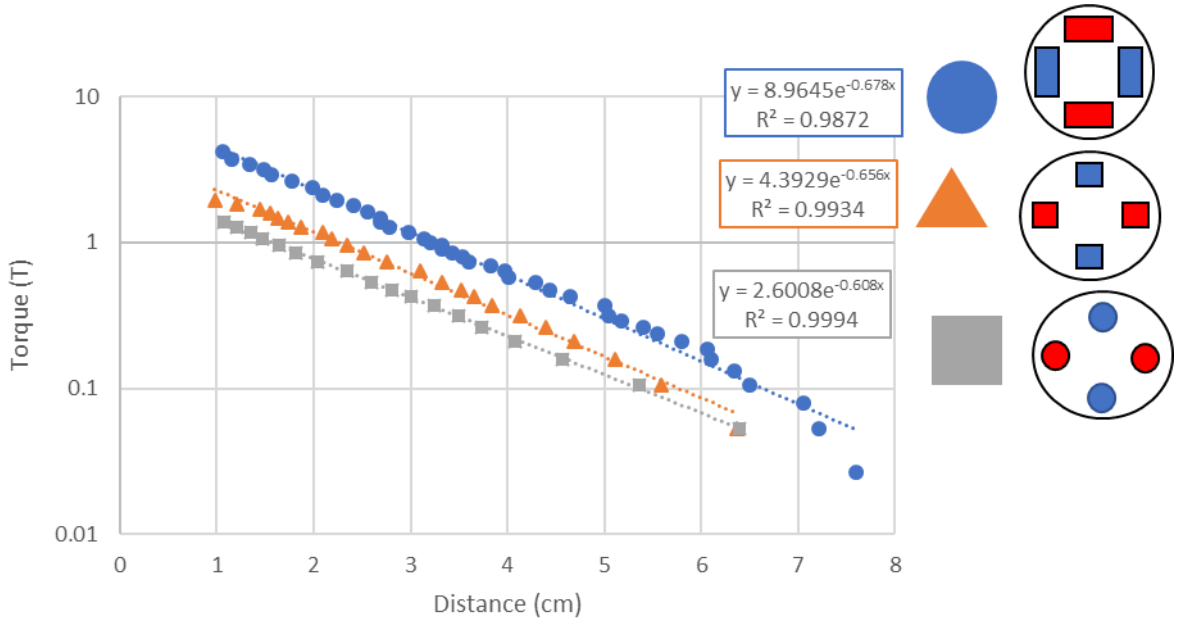

Figure 4.2. Maximum torque vs. separation for different types of magnets mounted in the couplers.

In this experiment, the variable B_r was initially thought to be varied due to the differences in pulling forces. After further investigation, of the magnets purchased, it was found that all the magnets have the same B_r.

Table 4.1. Specifications for each magnet used in this test

Magnets used	Grade	Pulling force	B_r (T)
Rectangle 2”x1”x0.5”	N50	87lbs	1.32
Square 1”x1”x0.5”	N55	55lbs	1.32
Round 1”d x 0.5”	ND 60	49lbs	1.32

Yet when given the same $B_{r,}$ the graphs did not come out the same. This is due to the geometries not being the same. The larger the magnets, the more surface area, and volume it takes up in the disc. This is further explored next.

4.3 Number of Magnets

To understand how the number of magnets would affect the relationships the same magnets were used. Figure 4.2 graphs display, how the number of magnets may affect the pull-out torque. Figure 4.2(a) displays the 1”x1”x0.5” square magnets on a 5.5” diameter disc. The darker the line gets, the more magnetic pairs that arrangement had in the housing. There is an added picture of the arrangements on the graph. The pictures of the arrangements on the discs from the top down have respectively related the lines on the graph. The blue lines go from 4 magnetic pairs to 6 magnetic pairs and then to 8 magnetic pairs. On graph (b), this shows the 0.5” cubed magnet. The dark blue line represents eight magnetic pairs while the light blue line represents four magnetic pairs. This graph has the same concept as above.

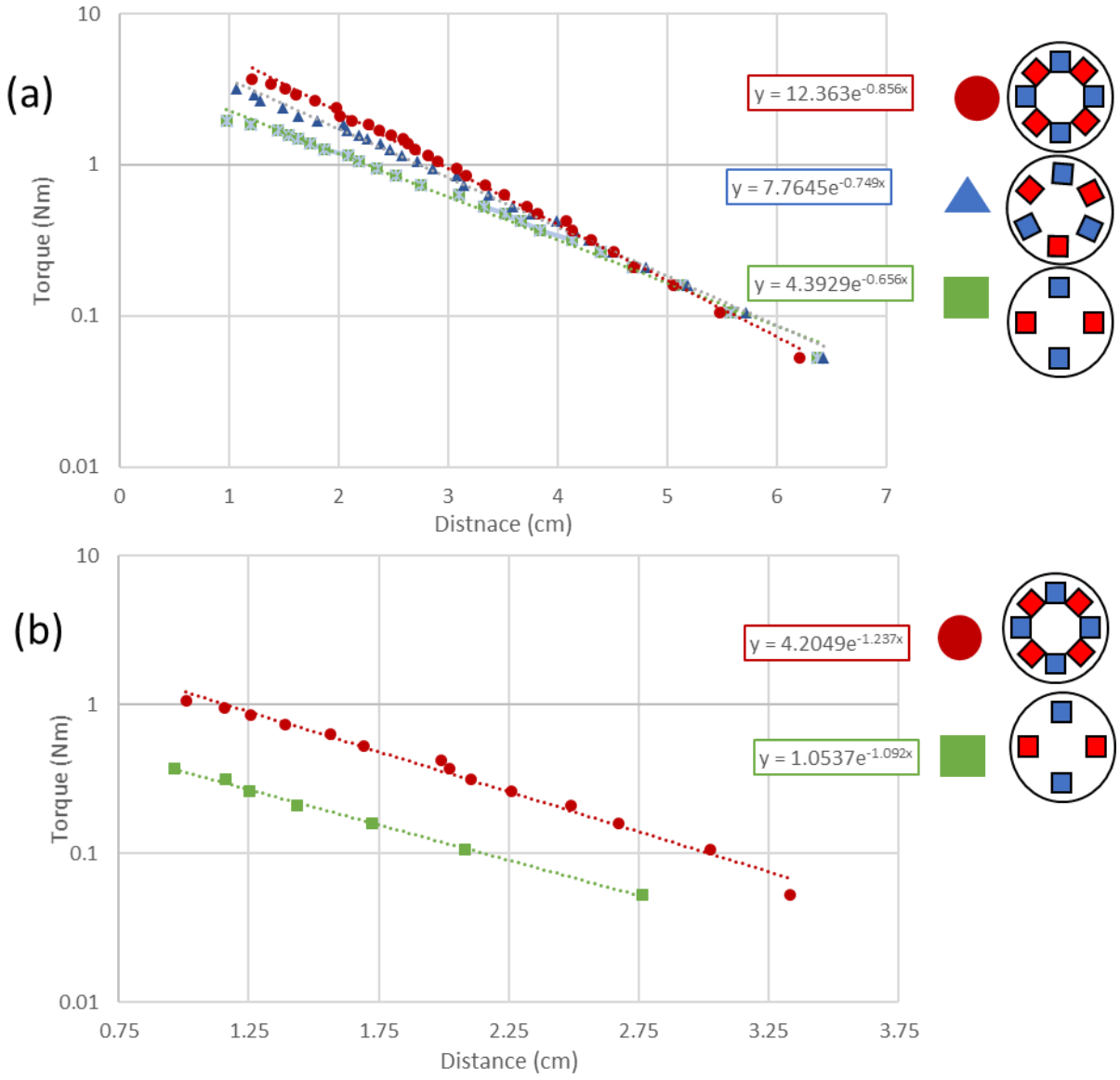

Figure 4.3. Graph (a) shows a varying number of 1" magnets (b) shows a varying number of 0.5" magnets. Both graphs are on a logarithmic y-axis.

We had noticed that the greater the number magnetic pairs there were, the stronger the pull-out torque was. Again, the best-fit equation, for these data follows Eq. 19. After looking at the graph 4.3a, we then began to look at the 'b' variable.

Table 4.2. experimental data for graph 4.3a.

8 magnets	6 magnets	4 magnets
b = .856	b = .749	b = .656

To prove that the experimental results were conclusive with the analytical models, the ratio between the 'b' values of the experimental model are then compared to the ratios of the 'k' values of the analytical models. This is because experimentally, the coefficient of x is -b, while the coefficient of x(ν) of our analytical model is -k(2h+x). This goes with the assumption of x=1, then $b \approx k$. The value k consists of the domains, D_x and D_y. The domain D_x is affected by the number of magnets, because the number of magnets will affect the equidistant arclength found at the radius to magnets center. The number of magnets is divided by 360° to get the theta between all the magnets.

The ratios of 'b' were found to compare to the ratios of 'k.' Both 'b' and 'k' are the coefficient to the airgap distance. If the experimental model compares with the theoretical model the ratios would be similar since the values would be increasing proportionally. Here, the three ratios that were looked at experimentally were: $b_8/b_4=1.3$, $b_6/b_4=1.14$, and $b_8/b_6=1.14$.

Next, the analytical model was used to find the various values of k. Table 4.3 displays the values that were received for each variable. First, the D_x was found by finding the corresponding arc length of each set of arrangement (figure 2.1). D_y was to remain constant for any arrangement with the same r_{mc}. From there, equation (6) was used to find w_n and w_m. Then equation (8) was used to find κ.

Table 4.3 Theoretical data for varying the number of dipole pairs and the k parameter

	8 magnets	6 magnets	4 magnets
D_x(cm)	3.49	4.65	6.98
W_n	.899	.675	.449
D_y(cm)	5.08	5.08	5.08
W_m	.618	.618	.618
κ	1.09	.915	.764

Once k was found, then the ratios between k were found: κ_8/κ_4=1.43, κ_6/κ_4=1.19, and κ_8/κ_6=1.19. This was promising and showed the experimental model compared to the analytical model.

4.4 Varying radial distances

To show this experiment, each test had four magnets. We then decreased the sizes of the housing to decrease the radial distance of the magnet from the center. Each test consisted of the 1”x1” x.5” square magnets. In figure 4.4, the graph shows the blue (circle) line being the 5.5” diameter housing; the orange (triangle) line shows 4” diameter housing.

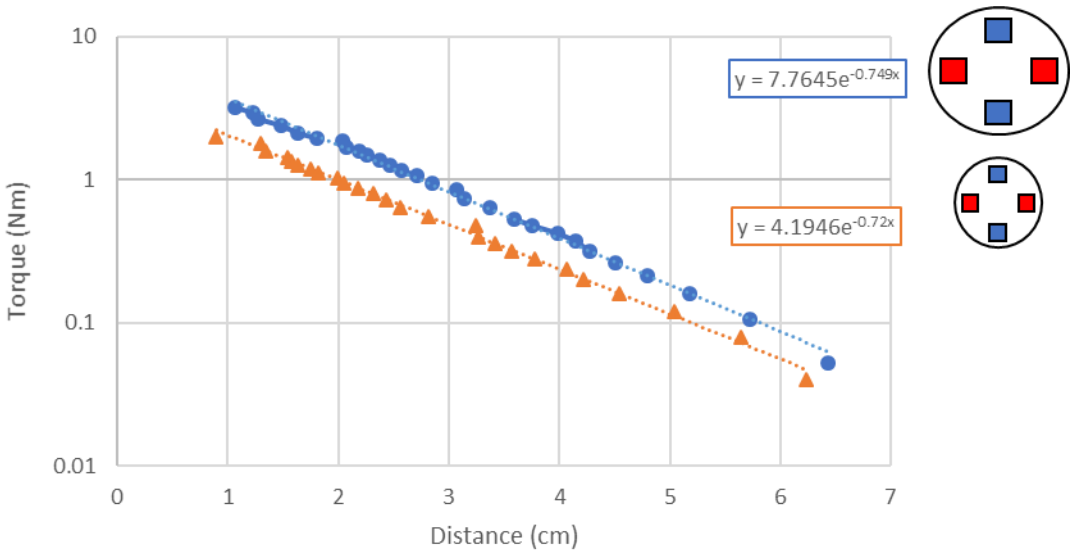

Figure 4.4. Pull out torque vs. air gap distance on different size magnetic couplers with the y-axis on a log scale.

In hindsight, it would have been beneficial to have the diameter of the housing the same, and only have the magnets move closer to the radius. From analyzing section 4.2, we learned that the geometry of the magnets has a strong influence on the torque. Unfortunately, the magnets in this experiment were downsized proportionality to the size of the frame. Because two varibles were changed simultaneously, this is potentially why the slopes of these lines are similar. Since everything was proportionally downsized, this includes the radius to the magnets center, overall frame radius and radius to the load, the exponent coefficient for each line should be similar and have the ratios between the two tests equal to one. The ratio between these experiments equal to .97.

Conclusion

After completing all the experiments, the experimental model of equation (19) can relate to that of the proposed theory in equation (18). After reviewing the analytical model, the parameters that might affect the graph of airgap vs. torque's shape were further explored, particularly k. The experiment found that the more dipole pairs, the stronger the couple would be. This also includes using as much of the housing as possible.

Some possible errors in the experiment may have contributed to the magnetic couple not being precisely parallel with one another. Any slight degree off would lower the efficiency, but not by much[7]. Another possible error would be attributed to having the motor side of the coupler being manually rotated, instead of having it on a motor and computationally monitoring the effects on the torque. This potentially would indicate that the tests might have given a lower value than what is ideally possible. However, when working with the magnetic couple, one would want to be well within the range of the maximum torque for whatever the installment may consist of.

For future work, to better the previous experiments, one would want to isolate as many variables as possible. For example, when testing strength, one would want to find magnets with the same geometry but different Br. Another example is one might use slots on the housing to adjust the magnets at various distances from the center. Different directions would be to explore other parameters of the final equation and find how it might relate to the simplified version. Other areas to test a magnetic coupler also include the efficiency of the magnetic coupler at various degrees off center. To include, one can test the efficiency of the magnetic coupler at various distances off center while keeping the couple parallel to one another.

Works Cited

[1] Disc, How, and Couplings Work. *Permanent Magnet Coupling This Two Piece Rare-Earth Permanent Magnet Coupling Is for Contact-Free Torque Transmission through Any Non-Ferrous Wall , with the Benefit of Slipping When the Maximum Torque Is Exceeded , Protecting Mechanical Components in The*. pp. 12–15.

[2] Dolisy, Bastien, Smail Mezani, et al. "A New Analytical Torque Formula for Axial Field Permanent Magnets Coupling." *IEEE Transactions on Energy Conversion*, vol. 30, no. 3, 2015, pp. 892–99, doi:10.1109/TEC.2015.2424159.

[3] Dolisy, Bastien, Thierry Lubin, et al. "Three-Dimensional Analytical Model for an Axial-Field Magnetic Coupling." *Progress In Electromagnetics Research M*, vol. 35, no. January, 2014, pp. 173–82, doi:10.2528/PIERM14031405.

[4] Fontchastagner, Julien, et al. "Design Optimization of an Axial-Field Eddy-Current Magnetic Coupling Based on Magneto-Thermal Analytical Model." *Open Physics*, vol. 16, no. 1, 2018, pp. 21–26, doi:10.1515/phys-2018-0004.

[5] Kosulin, Vladimir, and Irina Salova. *Calculation Features of Magnetic Coupling in Non-Magnetic Structures*. Vol. 01007, 2017, pp. 8–13.

[6] Lubin, T., et al. "Simple Analytical Expressions for the Force and Torque of Axial Magnetic Couplings." *IEEE Transactions on Energy Conversion*, vol. 27, no. 2, 2012, pp. 536–46, doi:10.1109/TEC.2012.2183372.

[7] Lubin, Thierry, et al. "Experimental and Theoretical Analyses of Axial Magnetic Coupling under Steady-State and Transient Operations." *IEEE Transactions on Industrial Electronics*, vol. 61, no. 8, 2014, pp. 4356–65, doi:10.1109/TIE.2013.2266087.

[8] Lubin, Thierry, and Abderrezak Rezzoug. "Improved 3-D Analytical Model for Axial-Flux Eddy-Current Couplings with Curvature Effects." *IEEE Transactions on Magnetics*, vol. 53, no. 9, 2017, doi:10.1109/TMAG.2017.2714628.

[9] "Steady-State and Transient Performance of Axial-Field Eddy-Current Coupling." *IEEE Transactions on Industrial Electronics*, vol. 62, no. 4, 2015, pp. 2287–96, doi:10.1109/TIE.2014.2351785.

[10] *Magnetic Coupling Boat*. https://www.kjmagnetics.com/blog.asp?p=magnetic-coupling. Accessed 6 May 2019.

[11] *Magnetic Couplings _ Magnetic Technologies Inc*. https://www.teausa.net/Latest-News/Post/631/Magnetic-Couplings. Accessed 6 May 2019

[12] Mei, Shunqi, et al. "Methods for Calculating the Transmission Torque of Magnetic Transmission Mechanisms." *IFIP International Federation for Information Processing*, vol. 207, no. 2005, 2006, pp. 631–36, doi:10.1007/0-387-34403-9_87.

[13] Nagrial, M. H., et al. "Design of Synchronous Torque Couplers." *World Academy of Science, Engineering and Technology*, vol. 5, no. 7, 2011, pp. 426–31.

[14] Östman, Andreas. *Force Measurements on Permanent Magnets and Demagnetization Effects of Assembling Halbach Arrays Demagnetization Effects of Assembling Halbach*. 2014.

[15] Post, Robert S., et al. *Permanent Magnet Coupling Fundamentals*. no. November, 1999, p. 1999.

[16] Ravaud, R., et al. "Torque in Permanent Magnet Couplings: Comparison of Uniform and Radial Magnetization." *Journal of Applied Physics*, vol. 105, no. 5, 2009, doi:10.1063/1.3074108.

[17] Seo, Sung Won, et al. "Analytical Torque Calculation and Experimental Verification of Synchronous Permanent Magnet Couplings with Halbach Arrays." *AIP Advances*, vol. 8, no. 5, 2018, doi:10.1063/1.5006731.

[18] Yonnset, J. P., et al. "Analytical Calculation of Permanent Magnet Couplings." *IEEE Transactions on Magnetics*, vol. 29, no. 6, 1993, pp. 2932–34, doi:10.1109/20.280913.

[19] Yu, Linxin, et al. "The Influence of Material on the Performance of Permanent Magnet Eddy Current Speed-Control Device." *Proceedings of the 29th Chinese Control and Decision Conference, CCDC 2017*, 2017, pp. 6858–63, doi:10.1109/CCDC.2017.7978415.

[20] "The Influence of Material on the Performance of Permanent Magnet Eddy Current Speed-Control Device." *Proceedings of the 29th Chinese Control and Decision Conference, CCDC 2017*, no. May 2018, 2017, pp. 6858–63, doi:10.1109/CCDC.2017.7978415.